Linear Free-Energy Analysis of Mercury(II) and Cadmium(II) Binding to Three-Stranded Coiled Coils†

Debdip Ghosh,‡ Kyung-Hoon Lee,‡ Borries Demeler,§ and Vincent L. Pecoraro*,‡

Department of Chemistry, University of Michigan, Ann Arbor, Michigan 48109-1055, and Department of Biochemistry, The University of Texas Health Science Center at San Antonio, San Antonio, Texas 78229-3900

Received April 12, 2005; Revised Manuscript Received June 9, 2005

ABSTRACT: Investigators have studied how proteins enforce nonstandard geometries on metal centers to assess the question of how protein structures can define the coordination geometry and binding affinity of an active-site metal cofactor. We have shown that cysteine-substituted versions of the TRI peptide series [AcG-(LKALEEK)$_4$G-NH$_2$] bind Hg^{II} and Cd^{II} in geometries that are different from what is normally found with thiol ligands in aqueous solution. A fundamental question has been whether this structural perturbation is due to protein influence or a change in the metal geometry preference. To address this question, we have completed linear free-energy analyses that correlate the association of three-stranded coiled coils in the absence of a metal with the binding affinity of the peptides to the heavy metals, Hg^{II} and Cd^{II}. In this paper, six new members of this family have been synthesized, replacing core leucine residues with smaller and less hydrophobic residues, consequently leading to varying degrees of self-association affinities. At the same time, studies with some smaller and longer sequenced peptides have also been examined. All of these peptides are seen to sequester Hg^{II} and Cd^{II} in an uncommon trigonal environment. For both metals, the binding is strong with micromolar dissociation constants. For binding of Hg^{II} to the peptides, the dissociation constants range from 2.4×10^{-5} M for Baby L12C to 2.5×10^{-9} M for Grand L9C for binding of the third thiolate to a linear $Hg^{II}(pep)_2$ species. The binding of Hg^{II} to the peptide Grand L9C is similar in energetics for metal binding in the metalloregulatory protein, mercury responsive (merR), displaying ∼50% trigonal Hg^{II} formation at nanomolar metal concentrations. Approximately, 11 kcal/mol of the $Hg^{II}(Grand\ L9C)_3^-$ stability is due to peptide interactions, whereas only 1−4 kcal/mol stabilization results from $Hg^{II}(RS)_2$ binding the third thiolate ligand. This further validates the hypothesis that the favorable tertiary interactions in protein systems such as merR go a long way in stabilizing nonnatural coordination environments in biological systems. Similarly, for the binding of Cd^{II} to the TRI family, the dissociation constants range from 1.3×10^{-6} M for Baby L9C to 8.3×10^{-9} M for TRI L9C, showing a similar nature of stable aggregate formation.

Metal ions are essential to all biological systems. Nature has harnessed the special properties that metals possess to perform a variety of functions commonly associated with life. The importance of these ions can be established from the fact that almost one-third of all naturally occurring proteins contain metal ions. The forces that influence the final metalloprotein structure can be placed between two limiting conditions: one where the metal coordination dictates the final geometry (e.g., zinc finger motifs) (*1*, *2*) and one in which the peptide scaffold defines the final structure (e.g., Cu-azurin protein) (*3*). In the former case, the protein is mostly unstructured in the apo form. Only in the presence of zinc is the signature $\beta_2\alpha$ fold of zinc finger proteins observed. In the case of azurin, the apoprotein fold is nearly identical to the copper-bound form. The structural constraints of the polypeptide backbone only stabilize the Cu^I oxidation level of this electron-transport protein. Considering these two limiting cases, considerable effort has been expended in studying the binding of metals to partially folded/unstructured, native, and *de novo* designed peptides, which influence their secondary conformations (*4*−*7*) and ultimately dictate the final structure. At the same time, the ability to design peptidic sequences that fold into predictable, stable secondary structures (without the aid of stabilizing factors such as disulfide bonds or metal-binding sites) and subsequently bind specified ligands and/or catalyze new reactions has also been pursued by many groups (*8*−*11*).

As an example where the polypeptide fold has been the determining factor in the overall structure of the metalloprotein, our group designed the amphipathic TRI family of peptides (Table 1) to study trigonal thiolato coordination environments for Hg^{II} and Cd^{II}, metals which prefer to adopt other geometries in aqueous solutions (*12*, *13*). To study metal-induced folding of proteins, our group designed two smaller members of the TRI family, two 23-residue peptides, Baby L9C and Baby L12C, which in the apo state were considerably unstructured. However, in the presence of Hg^{II},

† We acknowledge the National Institute of Health (5 R01 ES012236-02) for funding the research work conducted. The development of the UltraScan software was supported by NSF Grant DBI-9974819 awarded to B.D.

* To whom correspondence should be addressed. Telephone: (734) 763-1519. Fax: (734) 936-7628. E-mail: vlpec@umich.edu.

‡ University of Michigan.

§ The University of Texas Health Science Center at San Antonio.

10.1021/bi0506674 CCC: $30.25
Published on Web 07/13/2005

Table 1: List of Peptides and Their Sequences Used in the Study

peptides	sequences
Mini L9C	Ac-G LKALEEK **C**KALEEK G-NH_2
Baby L9C	Ac-G LKALEEK **C**KALEEK LKALEEK G-NH_2
Baby L12C	Ac-G LKALEEK LKA**C**EEK LKALEEK G-NH_2
TRI	Ac-G LKALEEK LKALEEK LKALEEK LKALEEK G-NH_2
TRI L9C	Ac-G LKALEEK **C**KALEEK LKALEEK LKALEEK G-NH_2
TRI V_aL_dL9C	Ac-G**V**KALEEK **C**KALEEK **V**KALEEK **V**KALEEK G-NH_2
TRI L2WL9C	Ac-G**W**KALEEK **C**KALEEK LKALEEK LKALEEK G-NH_2
TRI L9CL16A	Ac-G LKALEEK **C**KALEEK **A**KALEEK LKALEEK G-NH_2
TRI L16C	Ac-G LKALEEK LKALEEK **C**KALEEK LKALEEK G-NH_2
TRI L9AL16C	Ac-G LKALEEK **A**KALEEK **C**KALEEK LKALEEK G-NH_2
TRI L12VL16C	Ac-G LKALEEK LKA**V**EEK **C**KALEEK LKALEEK G-NH_2
TRI L12GL16C	Ac-G LKALEEK LKA**G**EEK **C**KALEEK LKALEEK G-NH_2
Grand L9C	Ac-G LKALEEK **C**KALEEK LKALEEK LKALEEK LKALEEK G-NH_2
heptad	*g a b c d ef g a b c d ef g a b cd e f g a b cd e f g a bc d e f g a*

they spontaneously folded into three-stranded coiled coils encapsulating Hg^{II} in a trigonal geometry (*14*, *15*). This present report has focused on the thermodynamic properties of metal binding by some of the members of this family of peptides. The results obtained clearly demonstrate that the final metallopeptide structure is governed by the inherent free energy of folding of the polypeptide chain. In this paper, several new members of this family have been introduced, each having varying degrees of association affinities. However, all of the peptides sequester Hg^{II} and Cd^{II} using a trigonal thiolato coordination mode, geometries which are not common in aqueous solutions but which can be found in metalloregulatory proteins such as mercury responsive (merR).[1] We use a linear free-energy correlation between the association preferences of the peptides in the apo state and in the presence of metals to assess the origin of the nonstandard metal coordination geometry. In the case of Hg^{II}, the fundamental driving force for trigonal geometry attainment is dependent on the structural constraints of the peptidic system. These studies have shown that, irrespective of whether the metal induces folding of unstructured peptides or the metals bind to structured peptides, the final structure is still governed by the polypeptide-folding preference. For Cd^{II}, the studies further underscore the fact that the protein tertiary structural requirements play a critical role in dictating the final geometry of the metal.

MATERIALS AND METHODS

Peptide Synthesis and Purification. All peptides were synthesized on an Applied Biosystems 433A peptide synthesizer by using standard protocols (*16*) and purified and characterized as described (*14*). The stock solution concentrations were determined by using the Ellman's test (*17*). A list of the peptides synthesized with their sequences is given in Table 1.

Circular Dichroism (CD) Spectroscopy. CD titrations were performed on an AVIV 14D spectrophotometer attached to a temperature control bath. Guanidinium hydrochloride titrations were performed using a Microlab 500 series automatic titrator (Hamilton Co.) controlled by AVIV-supplied software. The titrations were carried out by mixing two separate solutions of peptide (containing 0 and 8.6 M of GuHCl); refractive index measurements were used to determine the concentration of the guanidinium hydrochloride solution (*18*). Each solution contained about 1000 μM phosphate buffer solution and 5−10 μM peptide. The pH values of the solutions were adjusted to 8.5 using an Accumet gel-filled pencil-thin Ag/AgCl single-junction electrode with an Orion Research digital pH millivolt meter 611. Titrations were performed at 25 ± 1 °C in a 1 cm path-length rectangular quartz cell. The mean residue ellipticity at 222 nm was calculated using the relation $[\theta]_{222} = \theta_{obs}/(10lcn)$, where θ_{obs} is the observed ellipticity in millidegrees, l is the path length of the cell in centimeters, c is the peptide concentration in moles per liter, and n is the number of residues per peptide.

Analyses of the guanidinium hydrochloride titrations were performed to extract association affinities of the peptide coiled coils for each other by a previously described combined numerical and nonlinear least-squares fitting to the data (*12*, *14*, *19*). These calculations were performed using Matlab version 5.2.1 (The Mathworks, Inc.).

For the TRI chain of peptides and Grand L9C, a simple two-state model of three-stranded coiled-coil unfolding to the monomer upon addition of guanidinium hydrochloride was used to fit the data using the following relation to determine the dissociation constant K_{diss}

$$T \leftrightarrows 3M \qquad K_{diss} \tag{1}$$

where M = monomer, T = trimer, and $K_{diss} = [M]^3/[T]$.

For the shorter baby L9C and baby L12C peptides, the data were fit to a monomer−dimer−trimer equilibrium using the relation below to determine the two dissociation constants

$$T \leftrightarrows D + M \leftrightarrows 3M \qquad K_{diss2}, K_{diss1} \tag{2}$$

where M = monomer, D = dimer, T = trimer, $K_{diss1} = [M]^2/[D]$, and $K_{diss2} = [D][M]/[T]$.

Further information about the models has been provided in the Supporting Information.

UV−Vis Spectroscopy. Metal-binding titrations of the peptides with Hg^{II} were performed by titrating aliquots of a ~3 mM stock solution of peptide into a 2.5 mL solution containing 10 μM $Hg^{II}Cl_2$ and 50 mM phosphate buffer at pH 8.5 and monitoring the development of ligand−metal charge-transfer bands between 200 and 320 nm on a Carey 100 Bio UV−vis spectrophotometer. All solutions were purged with argon before titrations to minimize the chances of oxidation. For each addition of peptide, an equivalent addition was made in the background solution containing only 50 mM phosphate buffer so that the difference spectra taken could be attributed only to changes because of metal−

[1] Abbreviations: merR, mercury responsive.

peptide conformational changes. After each addition of aliquot, the solutions were left to equilibrate for 1−2 min in the case of the smaller baby peptides and 10 min for the TRI peptides before the reading was taken. For grand L9C, batch titration was performed where aliquots of peptide were added to 10 μM $HgCl_2$ and the solutions were left to equilibrate overnight inside a glovebag. Readings on these solutions were then taken the following day.

These titrations were analyzed using nonlinear least-squares fits of the absorbance as a function of the concentration of titrant added. Because of the extreme strength of the linear HgS_2 bond, stability constants could not be obtained for the 2:1 peptide/metal adduct. Fortunately, the binding constant for the addition of the third thiolate to $Hg(SR)_2$ was sufficiently weak to be measured by spectrophotometric titrations. Binding constants were estimated using a nonlinear least-squares analysis algorithm with MAPLE 7 and Kaleidagraph 3.0 (by Synergy Software) using the model

$$Hg^{II}(RS)_2 + RS^- \leftrightarrows Hg^{II}(RS)_3^- \qquad K_{bind} \qquad (3)$$

The pK_a for the step: $Hg^{II}(RS)_2HSR \leftrightarrows Hg^{II}(RS)_3^- + H^+$ was previously determined to be 7.6 ± 0.2 (*13*).

Further information about the model has been provided in the Supporting Information.

Metal-binding titrations of some of these peptides were also conducted with Cd^{II} using a similar method. The only difference was the use of 50 mM Tris buffer at pH 8.5 instead of phosphate buffer. These titrations were similarly analyzed using nonlinear least-squares fits of the absorbance as a function of the concentration of titrant added. The binding constant for binding of the peptide to Cd^{II} was determined using the model

$$Cd^{II} + (RS)_3^{3-} \leftrightarrows Cd^{II}(RS)_3^- \qquad K_{bind} \qquad (4)$$

The apparent pK_a for the step: $Cd^{II}(HSR)_3 \leftrightarrows Cd^{II}(RS)_3^- + 3H^+$ was previously determined to be 6.8 ± 0.2 (*13*).

Further information about the model has been provided in the Supporting Information.

Analytical Ultracentrifugation Studies. Sedimentation velocity and sedimentation equilibrium experiments were conducted on Hg^{II} complexes of the peptides baby L9C, TRI L9C, and grand L9C in phosphate buffer solutions (pH 8.5) to identify possible association states.

Sedimentation Velocity. A 0.9 OD 280 nm solution of each L9C peptide was sedimented at 20 °C and 60 krpm in 50 mM potassium phosphate buffer (pH 8.5) containing 150 mM KCl in 2-channel aluminum centerpieces in the AN-60 Ti rotor. A total of 150 absorbance scans were collected at 280 nm and analyzed by the method of van Holde−Weischet (*20*). The partial specific volume of each peptide was determined by the method of Durchschlag (*21*) from the protein sequence of each peptide and found to be 0.7644 cm^3m/g for baby L9C, 0.7687 cm^3m/g for TRI L9C, and 0.7714 cm^3m/g for Grand L9C. Data analysis was performed with the UltraScan software (*22*).

Sedimentation Equilibrium. For each peptide, 120 μL of six different loading concentrations (0.3, 0.5, and 0.7 OD 230 and 0.3, 0.5, and 0.7 OD 280) were sedimented to equilibrium at 20 °C at five different speeds (30, 35, 40, 45, and 50 krpm). To ensure a good signal from both the monomer and oligomeric species, it is important to span a large concentration range with the experimental data. This can be accomplished by varying the loading concentration and the wavelength of the measurement, which exploits the different extinction properties of the peptides. When data observed under multiple conditions are globally fit, such as multiple rotor speeds and multiple loading concentrations, it is possible to enhance the confidence in each fitted parameter value (*23*). Extinction coefficients for multiple wavelength measurements were determined by performing wavelength scans between 220 and 340 nm for each concentration and globally fitted to a global extinction profile using UltraScan (Figure 1). The extinction profile was normalized with the extinction coefficient at 280 nm by estimation from the protein sequence according to the method by Gill and von Hippel (*24*) and as implemented in UltraScan. The results are shown in Figure 2, and values for 230 and 280 nm are listed in Table 2. Equilibrium scans

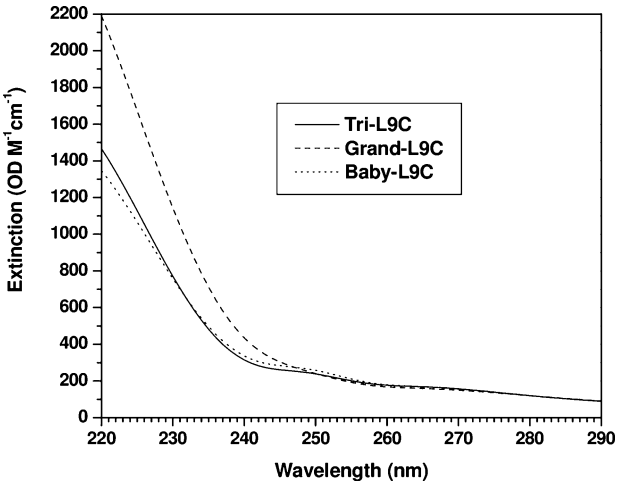

FIGURE 1: Extinction profile resulting from the global fit of the wavelength scans from the L9C peptides. Extinction coefficients from this fit were used to correct the equilibrium constants calculated in the global equilibrium analysis.

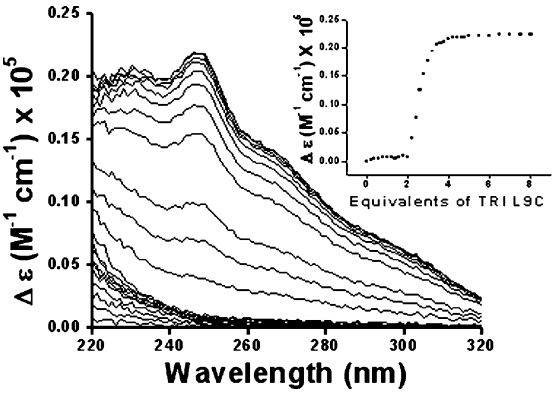

FIGURE 2: UV−vis titration of TRI L9C into a solution of $Hg^{II}Cl_2$ at pH 8.5. The data are plotted as $\Delta\epsilon$ versus wavelength. The inset shows the titration curve plotted as $\Delta\epsilon$ versus equivalents of peptide added at 247 nm.

Table 2: Extinction Coefficients for 230 and 280 nm as Determined for the L9C Peptides

peptide	E_{230} (OD mol^{-1} cm^{-1})	ϵ_{280} (OD mol^{-1} cm^{-1})
Baby L9C	758.2	120.0
TRI L9C	771.2	120.0
Grand L9C	1143.4	120.0

Table 3: Dissociation Constants (K_{diss}) for the Peptides from the Guanidinium Denaturation Experiments and Binding Constants (K_{bind}) for Binding of the Third Thiolate to Linear $Hg(RS)_2$ as Determined by Fits to the Data

peptide	K_{diss} (M^2)	$-\Delta G_{assoc}$[a] (kcal/mol)	m_g[b] (kcal/mol)	K_{bind} (M)	$-\Delta G_{bind}$ (kcal/mol)
Baby L12C	$\boldsymbol{K_{diss1}}$[c] $= 2.0 \times 10^{-4}$	5.0	0.6	4.1×10^4	6.3
	$\boldsymbol{K_{diss2}} = 2.0 \times 10^{-7}$	9.1	4.9		
Baby L9C	$\boldsymbol{K_{diss1}} = 1.2 \times 10^{-5}$	6.7	0.5	1.6×10^5	7.1
	$\boldsymbol{K_{diss2}} = 8.5 \times 10^{-9}$	11.0	5.0		
TRI L12GL16C	6.8×10^{-10}	12.5 (4.2)	0.8	5.2×10^5	7.8
TRI L9AL16C	4.1×10^{-10}	12.8 (4.3)	0.6	1×10^6	8.2
TRI L9CL16A	5.4×10^{-11}	14.0 (4.7)	0.8	1.2×10^6	8.3
TRI L12VL16C	3.2×10^{-11}	16.5 (5.5)	1.1	3.3×10^6	8.9
TRI L2WL9C	2.9×10^{-13}	17.1 (5.7)	2.6	4.7×10^6	9.1
TRI V_aL_dL9C	1.5×10^{-13}	17.5 (5.8)	1.6	1.1×10^7	9.6
TRI L16C	9.8×10^{-15}	19.1(6.4)	1.9	2.8×10^7	10.1
TRI L9C	5.9×10^{-15}	19.4 (6.5)	1.9	3.6×10^7	10.3
Grand L9C	1.3×10^{-18}	24.4 (8.1)	2.3	4.5×10^8	11.8

[a] The values of $-\Delta G_{assoc}$ within the parentheses are for a single monomer. The error per aggregate is 0.4 kcal/mol. [b] m_g quantifies the effect of guanidinium on the free energy of folding $\Delta G^0 = \Delta G^0_{0M} - m_g$[GuHCl], where ΔG^0_{0M} is the free energy of folding of the peptide in the absence of guanidinium hydrochloride. [c] The guanidinium denaturation data for the peptides, Baby L9C and Baby L12C, were fit using a monomer−dimer−trimer equilibrium as described by the equation: $T \leftrightarrows D + M \leftrightarrows 3M$; K_2, K_1.

Table 4: Dissociation Constants (K_{diss}) for the Peptides from the Guanidinium Denaturation Experiments and Binding Constants (K_{bind}) for Binding of Thiolates to Cd^{II} as Determined by Fits to the Data

peptide	K_{diss} (M^2)	$-\Delta G_{assoc}$[a] (kcal/mol)	m_g[b] (kcal/mol)	K_{bind} (M)	$-\Delta G_{bind}$ (kcal/mol)
Baby L9C	$\boldsymbol{K_{diss1}}$[c] $= 1.2 \times 10^{-5}$	6.7	0.5	7.7×10^5	8.0
	$\boldsymbol{K_{diss2}} = 8.5 \times 10^{-9}$	11.0	5.0		
TRI L9AL16C	4.1×10^{-10}	12.8 (4.3)	0.6	7.0×10^6	9.3
TRI L9CL16A	5.4×10^{-11}	14.0 (4.7)	0.8	2.7×10^7	10.1
TRI L12VL16C	3.2×10^{-11}	16.5 (5.5)	1.1	3.2×10^7	10.2
TRI L2WL9C	2.9×10^{-13}	17.1 (5.7)	2.6	8.8×10^7	10.8
TRI L9C	5.9×10^{-15}	19.4 (6.5)	1.9	1.2×10^8	11.0

[a] m_g quantifies the effect of guanidinium on the free energy of folding $\Delta G^0 = \Delta G^0_{0M} - m_g$[GuHCl], where ΔG^0_{0M} is the free energy of folding of the peptide in the absence of guanidinium hydrochloride. [b] The values of $-\Delta G_{assoc}$ within the parentheses are for a single monomer. The error per aggregate is 0.4 kcal/mol. [c] The guanidinium denaturation data for the peptides, Baby L9C, were fit using a monomer−dimer−trimer equilibrium as described by the equation: $T \leftrightarrows D + M \leftrightarrows 3M$; K_2, K_1.

were taken with 0.001 cm radial increments and 20 averages. Sedimentation was performed in six-channel epon/charcoal centerpieces. The resulting data were globally analyzed with UltraScan by fitting to multiple noninteracting and self-associating models.

RESULTS

CD Spectroscopy. The association affinities (K_{diss}) in the absence of metal of all of the peptidic coiled coils used in this research was determined by monitoring the change in the CD signal at 222 nm, the typical α-helical signature, upon addition of guanidinium hydrochloride. The titration data were analyzed using a combined numerical and least-squares fitting procedure to obtain the free energy of coiled-coil formation (*12*, *14*, *19*), and the values are reported in Table 3. An increase in the length of the peptide by one heptad to form Grand L9C resulted in a greater number of hydrophobic contacts in the core, causing a significant rise in the association affinities, with the free energy of folding increasing by about 5 kcal/mol per coiled-coil aggregate relative to TRI L9C. The data further indicate that systematic replacement of a leucine residue in the TRI L16C peptides for smaller and less hydrophobic residues such as valine, alanine, and glycine results in a systematic disruption of the core hydrophobic affinity, giving rise to a weaker association of the peptides for each other (∼1−2 kcal/mol per residue per peptide). A similar effect is observed for the TRI L9C peptides with a decrease in stability on the replacement of core hydrophobic residues.

For the smaller Baby L9C and Baby L12C peptides, however, the data indicated the presence of more than two species and the data could be best fit to a monomer−dimer−trimer model as indicated in eq 2.

UV−Vis Spectroscopy. The trigonal complex, $Hg(SR)_3^-$, displays a very characteristic ligand−metal charge-transfer signature at 247 nm at pH 8.5 as shown in Figure 2, which is however not displayed at [peptide]/[$HgCl_2$] ≤ 2. Corresponding to the association affinities of the peptides as seen with CD studies, the binding affinities of all of the peptides for Hg^{II} followed a similar pattern. Thus, while titration of Grand L9C into $HgCl_2$ was seen to achieve about 99% of the maximum signal by 3 equiv, Baby L9C needed as much as 6 equiv to display similar absorption limits signifying a stronger affinity of the longer and more hydrophobic Grand L9C peptide for Hg^{II} compared to the comparatively unstructured Baby L9C. These binding preferences are consequently reflected in the binding strengths (Table 3). Similar patterns are observed for all of the peptides undertaken in this study.

Similar to the observed spectra for Hg^{II} titration, the $Cd(SR)_3^-$ moiety displays a characteristic ligand−metal charge transfer at 235 nm at pH 8.5. However, unlike the Hg^{II} system, the development of this trigonal species was consistently observed from the very beginning of the titration (see Figure S1 in the Supporting Information). Stability constants for Cd^{II} binding to these peptides are noted in Table 4.

Analytical Ultracentrifugation Study: Sedimentation Velocity. The van Holde−Weischet analysis resulted in a half-

Table 5: Results of Global Fits to the Analytical Ultracentrifugation Data Collected on the Peptides

peptide	best-fit model	monomer MW	variance	dissociation constant (K_d)
Baby L9C	monomer−dimer−tetramer	2.61 kD (2.56 kD)[a]	1.2135×10^{-5}	$K_{1,2}$, 36.6 μM; $K_{1,4}$, 112.3 μM
TRI L9C	monomer−trimer	3.80 kD (3.37 kD)	7.2096×10^{-6}	$K_{1,3}$, 127.3 μM
Grand L9C	monomer−trimer	4.55 kD (4.18 kD)	1.1020×10^{-5}	$K_{1,3}$, 44.7 μM

[a] The values within parentheses represent the expected molecular weights, while those on the outside are the experimentally observed ones.

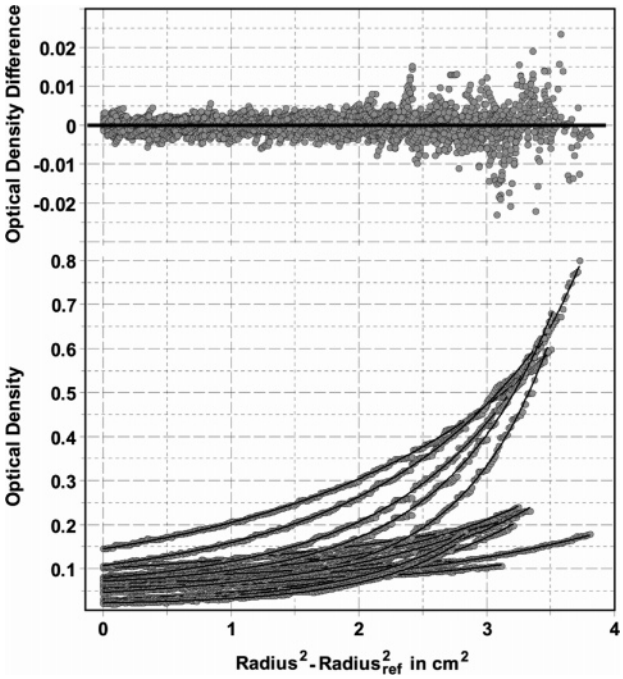

FIGURE 3: Residuals (top) and overlays (bottom) of a global fit of the experimental equilibrium data measured at 230 and 280 nm from the Tri-L9C peptide to a reversible self-associating monomer−trimer model.

parabola-shaped sedimentation coefficient distribution for all peptides, ranging between 0.8 and 1.5 s, with a weight average sedimentation coefficient of 1.24 s for Baby L9C, 1.36 s for TRI L9C, and 1.31 s for Grand L9C. The shape of this sedimentation coefficient distribution is indicative of self-association behavior (*25*).

Sedimentation Equilibrium. For all peptides, the analysis revealed the presence of multiple species with different molecular weight, and a two-component, ideal, noninteracting model provided the best fit to the data as judged by the variance and the residual run patterns. When the penalty of fewer degrees of freedom is taken into account in a self-associating model (where the molecular weight for all species is constrained to be an integral multiple of the monomeric molecular weight and the partial concentration of each species is constrained by the equilibrium constant), such constrained models resulted in only marginally increased variance, indicating that self-association models are more appropriate for the description of the system. The results from the global fitting are summarized in Table 5, and a representative fit of the TRI L9C peptide to a monomer−trimer reversibly self-associating model is shown in Figure 3. Relative distributions of self-associating oligomeric species as a function of the concentration are shown in Figures S2−S4 in the Supporting Information). For the longer TRI L9C and Grand L9C peptides, the analytical ultracentrifugation results indicated that the data were entirely consistent with a monomer−trimer model in the presence of Hg^{II} at pH 8.5. For the smaller Baby L9C peptide, analytical ultracentrifugation results indicate that when the data were fit using a monomer−dimer model (two-component, noninteracting model), the monomer molecular weight is very close to the correct dimer molecular weight but the variance is a little high, which is not very significant, considering that there are fewer degrees of freedom in a two-component model than in a three-component model. On the other hand, the monomer−trimer model (also a two-component noninteracting model) has a significantly higher variance and a higher monomer molecular weight, which argues that it is not as good of a representation of the data. To resolve this problem, a three-component model was used to fit the data. The monomer−dimer−trimer model gave a low variance, but the monomer molecular weight deviated significantly from the known value (monomer molecular weight = 2598). However, on using a monomer−dimer−tetramer model, the fittings gave the best variance and a reasonable monomer molecular weight.

The discrepancies about the aggregation state of the coiled coils that arise out of the two techniques, UV−vis spectroscopy and analytical ultracentrifugation spectroscopy, have been clarified in the following section.

DISCUSSION

The driving force to form a linear Hg−bis(thiolate) bond is very high ($\Delta G = -78$ kcal/mol). On the contrary, with cysteine, there is a significantly weaker preference for binding a third thiolate to a linear, bis(thiolate)Hg^{II} complex (~ -1.2 kcal/mol) (*26*). Considering a solution containing 1 μM Hg^{II} and 10 μM RS^- (where R refers to any linear organic group), less than 0.001% Hg would be in a trigonal thiolate form. At the low concentrations found in cells, Hg^{II} would prefer to be linear and two coordinate. Nearly 1 M RS^- ligand is required to have $Hg(SR)_3^-$ as the significant complex in aqueous solution.

Given these inherent binding preferences, it is remarkable that the metalloregulatory protein, merR, sequesters Hg^{II} in a trigonal structure at nanomolar concentrations (*27*, *28*). The driving force for this unusual coordination environment for Hg probably stems from the ability of the protein to orient itself in a favorable manner for three ligands to be in very close proximity to each other and to Hg. We had previously predicted that, if we could build a large negative free energy of folding into a three-stranded coiled coil, then this association energy would be able to perturb the cysteine-like equilibrium, allowing us to isolate a trigonal thiolato−Hg^{II} at stoichiometric metal/peptide ratios (*12*, *14*). If successful, we would obtain a significant understanding of the energetics of the Hg^{II} binding to merR. Our hypothesis was that the associative affinity of the peptide subunits would overcome the metal preference at micromolar concentrations for linear coordination.

Our group had previously studied the thermodynamic implications of metal binding to the TRI family of peptides. This set of peptides is based on a 30 amino acid sequence, Ac-G-(LKALEEK)$_4$-G-NH_2, acetylated at the N terminus and amidated at the C terminus. This design included a heptad repeat unit with hydrophobic residues in the "*a*" and "*d*" positions of the heptad, a normal pattern for most α-helical peptides and proteins found in nature. Substitution of a leucine for a cysteine in the hydrophobic core resulted in a soft metal-binding site capable of binding to heavy metals such as Hg^{II} (*12*), Cd^{II} (*13*), Pb^{II} (*29*), and As^{III} (*30*). However, this singly mutated peptide showed a lower association affinity for itself than the former. Similarly, removal of a heptad from the sequence gave rise to peptides with a fewer number of hydrophobic contacts, resulting in significantly weaker affinity for aggregation (*14*, *15*). However, these peptide still gave rise to the formation of a trigonal thiolato−Hg^{II} complex.

We are frequently asked about the importance of the driving force for peptide aggregation on the final coordination number of the sequestered metal. Is it possible for any thiolate species to form a trigonal Hg^{II} complex with the metal, or is it the aggregation properties of the designed system that dictate the overall existence and stability of the final complex? Is it possible for Hg^{II} bound in a linear fashion to two thiolates to easily bind to a third sulfur presented by any exogenous ligand in solution to form trigonal species in a stoichiometric ratio? Last, in designed peptidic systems, how would the association affinity of the peptides for themselves, in the absence of a metal, be related to the binding affinities of the peptides with the metal? Our research in this paper has answered these questions.

The presented data support our contention that it is the self-aggregation of the three-stranded coiled coils that drives the formation of the trigonal Hg(TRI LXC)$_3^-$ species To address the first point, two thiolate entities were used: one being a smaller member of the TRI family of peptides but having only two heptad repeats in the sequence instead of four (named Mini L9C) and the other being a small nonpeptidic thiol ligand, β-mercaptoethanol. Titration of β-mercaptoethanol into a solution of 10 μM $Hg^{II}Cl_2$ solution at pH 8.5 indicated that even addition of a large excess amount (∼500-fold) of β-mercaptoethanol failed to realize the trigonal Hg(SR)$_3^-$ species. This confirms that the simple presence of a thiol-donating ligand is not the sole criteria for the formation of trigonally coordinated Hg^{II}. The small peptide (Mini L9C) because of very few hydrophobic contacts is considerably less structured than the parent TRI L9C and consequently has a very small free energy of folding (∼0.5 kCal/mol). Similar to the previous observation with β-mercaptoethanol, this peptide also failed to form a trigonal Hg(Mini L9C)$_3^-$ species even at a 100-fold excess of peptide to $Hg^{II}Cl_2$ solution at pH 8.5. These observations clearly indicated that not only were smaller ligand systems incapable of forming a trigonal Hg^{II} structure at these concentrations, but even in peptidic systems, a significant amount of aggregation affinity is an important requirement for this reaction to proceed.

The important question that then needs to be addressed is what is the aggregation state of the TRI family of peptides in the association? For the longer TRI chain of peptides and for Grand L9C, analytical ultracentrifugation studies consistently prove that, at pH 8.5, the aggregation state is predominantly that of a three-stranded coiled coil in the apo state (*31*) as well in the metalated state (*vide supra*). This result is consistent with the other spectroscopic observations, which indicate the formation of a trigonal Hg^{II} charge-transfer band at 247 nm at pH 8.5. For the smaller baby L9C peptide, however, there is some discrepancy between the analytical ultracentrifugation data and the spectroscopically derived association model. The equilibrium ultracentrifugation results are best interpreted by a three-state model, monomer−dimer−tetramer, whereas the fits to the spectroscopic observations are described with a monomer−dimer−trimer model. A similar result is observed with the guanidinium denaturation results for the apo-baby L9C. The data fail to fit when one utilizes a monomer−trimer, two-component model. However, a good fit is obtained with a monomer−dimer−trimer model. It is not surprising that the folding process for Baby L9C is more complex than for TRI L9C because the smaller Baby L9C peptide has a significantly smaller free energy of folding. When closely looking at the results from the guanidinium experiments, it also indicates that the concentration of trimers in the mixture is close to ∼90%, while the concentration of dimers, though very small, is still significant enough to impact the fit. Guanidinium denaturation experiments with Baby L9C in the presence of $HgCl_2$ show a similar result. Fits to the data still conform to a three-component monomer−dimer−trimer model with the trimer concentration still close to 90%. Perhaps the best way to address this discrepancy between the analytical ultracentrifugation and spectroscopic studies is to say that both of these techniques strongly support the existence of more than two aggregation states; in other words, the fits to the data in both cases conform to three-state models. However, it must still be noted that the different techniques do give rise to some ambiguity in higher aggregation preferences.

To test if the association affinities of the designed peptides for themselves in the absence of a metal are directly proportional to the binding affinities of the peptides with the metal, a variety of peptides were synthesized, either by varying the chain length of the strand or by substituting smaller hydrophobic residues in the core, thereby altering the hydrophobic core affinity. Alterations in the hydrophobic affinity of the peptide strands for each other give rise to a chain of peptides that become consistently weaker in their ability to form a bundle, directly depending on the mutated residue. At the same time, the trigonal Hg^{II} binding constant for the addition of the third thiolate also linearly decreases. A linear free-energy plot (Figure 4) of the free energy of aggregation of the three-stranded coiled coils in the absence of metal with the free energy of the binding constants for the binding of the third thiolate to $Hg^{II}(pep)_2$ clearly indicates that the peptide/metal binding strength is directly correlated with the aggregation strength of the peptide. This is another indicator that trigonal Hg^{II} formation is due to the large negative free energy of folding built into the three-stranded coiled coil, which allow us to isolate a trigonal thiolato−Hg^{II} at stoichiometric peptide/metal ratios.

A closer look at the plot clearly clarifies two prior conflicts. First, for the smaller Baby L9C and Baby L12C peptides, the aggregation modes in their apo conditions have been considered as trimers and not as tetramers. In doing so, they seem to correlate very well with the other members

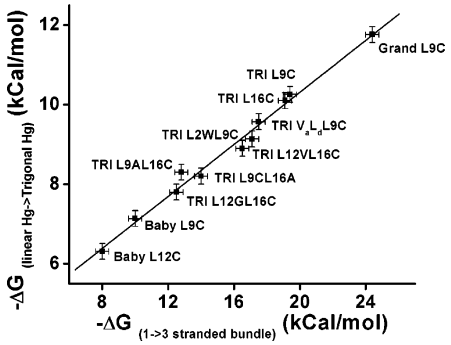

FIGURE 4: Figure showing a linear free-energy correlation between folding preferences of the peptides in the absence of metal to the binding of a third strand of peptide to a divalent $Hg^{II}S_2$ species.

of the TRI family. This further justifies our preference for a trimeric model for the smaller, weakly associated peptides. Second, the plot also explains the reason for the inability to form a trigonal Hg^{II} site with the two-heptad peptide, Mini L9C. The free energy for binding of the third thiolate decreases by about 3 kcal/mol on going from TRI L9C to Baby L9C (10 → 7 kcal/mol, refer to Table 3). At the same time, however, the free energy for aggregation of the bundle in the absence of a metal falls by ~9 kcal/mol per peptide. If we assume that a similar decrease would be seen for the loss of one more heptad in Mini L9C, then the free energy for bundle formation would be ~1 kcal/mol. However, this would be much lower than the energy that would be needed at these concentrations to form a trigonal Hg^{II} (~4 kcal/mol), assuming a similar decrease in affinity toward trigonal Hg^{II}. Hence, the weak and self-unassociated state of Mini L9C prevents isolation of a trigonal Hg^{II} moiety, giving further credibility to the fact that a certain degree of aggregation affinity is essential for the generation of a trigonal Hg^{II} species in stoichiometric amounts.

The validity of this free-energy analysis is supported further by similar analyses of the inherent $Hg(SR)_2 + RS^-$ free energy. Using ^{13}C NMR studies, Cheesman et al. determined complex formation constants for the formation of three-coordinate aqueous Hg^{II} complexes with L-cysteine, glutathione, and D,L-penicillamine at millimolar concentrations of $Hg(NO_3)_2$ (0.05−0.067 M) over the pH range of 8.65−9.36 (*32*). Their reported values for the free energies of complex formation, −1.2 kcal/mol for cysteine, −4.2 kcal/mol for glutathione, and −4.8 kcal/mol for penicillamine, indicated that a significant concentration of trigonal Hg^{II} was formed. In fact, for glutathione, it was seen that almost 50% of the Hg^{II} from a solution containing 1×10^{-3} M Hg^{II} and 7×10^{-3} M glutathione at pH 8.0 would be found as the $Hg(RS)_3^-$ species under physiological conditions. Shoukry et al. further studied these complexes using polarimetry and obtained similar formation constants (*33*). The extrapolation of our free-energy correlation to $\Delta G = 0$ kcal/mol for the association of the unmetalated peptides provides an estimate for the free energy of trigonal thiolate formation in the absence of stabilizing protein interactions. We obtain a value of −3.6 (1) kcal/mol, a value that is in remarkably good agreement with the independent experimental determinations. This observation both validates our free-energy analysis and also underscores the importance of the protein self-association affinity for the formation of the trigonal thiolato complex. Approximately, 7−10 kcal/mol of the Hg(TRI L9C)$_3^-$ stability is due to peptide interactions, whereas only 1−4 kcal/mol stabilization results from $Hg^{II}(RS)_2$ binding the third thiolate ligand. Effectively, our designed proteins (as well as merR) use the strategy of increasing the effective molar volume of thiolate ligands around Hg^{II} to achieve the desired coordination geometry.

To gain a better perspective of how the metal-bound active site of the TRI family of peptides compares with the active site of the metalloregulatory protein, merR, we decided to compare the energetics of the two systems. O'Halloran et al. observed using gel-shift assays that the metaloregulatory protein, merR, possesses nanomolar mercuric ion sensitivity (*27*, *28*). In comparison with the binding of Hg^{II} to Grand L9C at pH 9.0, where the cysteines are assumed to be completely deprotonated ($pK_a = 7.6$), about 50% of trigonal Hg^{II} is formed at ~5 nM concentrations. This affinity is remarkably similar with the natural protein system. It should be noted that, in the Hg(Grand L9C)$_3^-$ system, about ~11 kcal/mol energy is provided by the tertiary protein interactions toward the formation of the trigonal Hg^{II}. Thus, it is likely that a similar amount of free energy is required in the merR system to enforce the trigonal structure.

This correlation of association affinities of the peptides for each other with the trigonal coordination environment of Hg^{II} is, however, still under a limiting condition. Due to the extreme strength of the linear Hg−thiolate bonds, estimation of the total binding strength of the metal with the apopeptide is not feasible. As a result, the linear free-energy plot can only be related to the binding of a third thiolate to a divalent metal−peptide species with the formation of a trigonal Hg^{II} species.

To probe complete formation constants for metal binding to the peptides, we chose to look at Cd^{II} complexation, which we had shown bound to the TRI family of peptides (*13*, *34*). Cd^{II} binding demonstrated pH-dependent behavior from the metal−peptide aggregates showing an apparent pK_a of 7.0 ± 0.2. At pH 8.5, where >99% thiols were expected to be deprotonated, metal-binding titrations showed that Cd^{II} was bound to three sulfurs of the coiled coils. ^{113}Cd NMR, ^{111m}-Cd perturbed angular correlation spectroscopy, and EXAFS studies clearly indicated the generation of a mixture of two species: a trigonal $Cd-S_3^-$ and a distorted tetrahedral $Cd-S_3(H_2O)$ moiety. The relative proportion of these different structures depends on the substitution pattern (i.e., "*a*" versus "*d*"). This knowledge thus allowed us to investigate the linear free-energy correlation study with this system and verify whether the previous results of the Hg^{II} system were indeed a reflection of the self-association affinity of the peptides. Also, in this case, the estimated metal−peptide binding constant would not be under limiting conditions but in fact would be an estimate of the entire metal−peptide bundle binding strength. This would thus lend better support to our theory that the free energy of folding of the peptides/proteins is oftentimes the determining factor for generation and stabilization of an unusual coordination environment around a metal in most biological systems.

Cd^{II} metal-binding titrations with the peptides were conducted at pH 8.5. Unlike the Hg^{II} system, estimation of the total metal−peptide binding affinity to all three helices of the peptide was feasible. As was seen with the Hg^{II} system, the binding of the peptides with Cd^{II} directly correlated with the self-association of the apopeptides, with the stronger

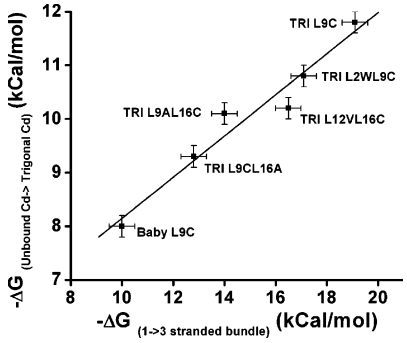

FIGURE 5: Figure showing a linear free-energy correlation between folding preferences of the peptides in the absence of metal to the binding of the peptides to $Cd^{II}Cl_2$.

affinity of peptides giving rise to stronger metal−peptide binding constants. A linear free-energy plot (Figure 5) for binding of some of these peptides with Cd^{II} showed an identical nature to the previous observation with the Hg^{II} system. The plot again further indicated that the affinity of bundle formation of the apopeptide dictated the final geometry and coordination environment around the central metal ion.

CONCLUSION

In this paper, we have examined the importance of polypeptide folding preferences in defining uncommon metal coordination geometries. A linear free-energy correlation study involving self-association affinity of the peptides versus binding affinity of the peptides to the heavy metals, Hg^{II} and Cd^{II}, has been presented. We have shown that cysteine-substituted versions of the TRI peptide series [AcG-$(LKALEEK)_4$G-NH_2] sequester Hg^{II} and Cd^{II} in geometries that are rare in aqueous solutions. In the case of Hg^{II}, the results clearly show that the fundamental driving force for trigonal geometry attainment is unambiguously dependent on the structural constraints of the ligand system. Thus, smaller ligands are seen to be incapable of forming a trigonal Hg^{II} moiety at micromolar concentrations, and even in peptidic systems, a significant amount of aggregation affinity is an important requirement for this reaction to proceed. The linear free-energy correlation further shows that the origin of this coordination geometry is also directly dependent on the degree of association affinity of the polypeptide. In the case of Cd^{II}, the studies further underline the importance of protein tertiary structural preferences in dictating the final geometry of the metal. Even though, in the case of Cd^{II}, there seems to be formation of a mixture of trigonal ($Cd^{II}S_3^-$) and tetrahedral [$Cd^{II}S_3(H_2O)$] entities, the final structure is still influenced by the protein fold. We conclude form our studies that perturbation of the geometry of Hg^{II} from two to three coordinate in designed peptides or merR requires a small energetic change, whereas the corresponding coordination geometry alteration of Cd^{II} from four to three coordinate requires a significant energetic penalty.

ACKNOWLEDGMENT

The authors thank Dr. Tsu-Chien Weng and Dr. Olga Iranzo for helpful discussions and Prof. Carin Stamper and Joshua Hays for helping collect analytical ultracentrifugation data at the Keck Biophysics facility at Northwestern University.

SUPPORTING INFORMATION AVAILABLE

CD spectroscopy, UV−vis spectroscopy, UV−vis titration curve (Figure S1), equilibrium distribution of the monomer and trimer species of grand L9C as a function of the total concentration (Figure S2), and equilibrium distribution of the monomer and trimer species of TRI L9C as a function of the total concentration (Figure S3). This material is available free of charge via the Internet at http://pubs.acs.org.

REFERENCES

1. Berg, J. M., and Godwin, H. A. (1997) Lessons from zinc-binding peptides, *Annu. Rev. Biophys. Biomol. Struct. 26*, 357−371.
2. Krizek, B. A., Amann, B. T., Kilfoil, V. J., Merkle, D. L., and Berg, J. M. (1991) A consensus Zinc finger peptide: Design, high affinity metal-binding, a pH-dependent structure, and His to Cys sequence variation, *J. Am. Chem. Soc. 113*, 4518−4523.
3. Randall, D. W., Gamelin, D. R., Lacroix, L. B., and Solomon, E. I. (2000) Electronic structure contributions to electron transfer in blue Cu and Cu_A, *J. Biol. Inorg. Chem. 5*, 16−19.
4. Ghadiri, M. R., and Choi, C. (1990) Secondary structure nucleation in peptides. Transition metal ion stabilized α-helices, *J. Am. Chem. Soc. 112*, 1630−1632.
5. Ghadiri, M. R., Soares, C., and Choi, C. (1992) Design of an artificial four helix-bundle metalloprotein via a novel ruthenium-(II) assisted self-assembly process, *J. Am. Chem. Soc. 114*, 4000−4002.
6. Lieberman, M., Tabet, M., and Sasaki, T. (1994) Dynamic structure and potential-energy surface of a 3-helix bundle protein, *J. Am. Chem. Soc. 116*, 5035−5044.
7. Kohn, W. D., Kay, C. M., Sykes, B. D., and Hodges, R. S. (1998) Metal ion induced folding of a *de novo* designed coiled-coil peptide, *J. Am. Chem. Soc. 120*, 1124−1132.
8. Ogawa, M. Y., and Kozlov, G. V. (1997) Electron transfer across a peptide−peptide interface within a designed metalloprotein, *J. Am. Chem. Soc. 119*, 8377−8378.
9. Federova, A., Chaudhari, A., and Ogawa, M. Y. (2002) Photon-induced electron-transfer along α-helical and coiled coil metallopeptides, *J. Am. Chem. Soc. 125*, 357−362.
10. Choma, C. T., Lear, J. D., Nelson, M. J., Dutton, P. L., Robertson, D. E., and DeGrado, W. F. (1994) Design of a heme-binding four-helix bundle, *J. Am. Chem. Soc. 116*, 856−865.
11. Robertson, D. E., Farid, R. S., Moser, C. C., Urbauer, J. L., Mulholland, S. E., Pidikiti, R., Lear, J. D., Wand, A. J., Degrado, W. F., and Dutton, P. L. (1994) Design and synthesis of multi-haem proteins, *Nature* 368, 425−432.
12. Dieckmann, G. R., McRorie, D. K., Tierney, D. L., Utschig, L. M., Singer, C. P., O'Halloran, T. V., Penner-Hahn, J. E., DeGrado, W. F., and Pecoraro, V. L. (1997) *De novo* design of mercury-binding two- and three-helical bundles, *J. Am. Chem. Soc. 119*, 6195−6196.
13. Matzapetakis, M., Farrer, B. T., Weng, T.-C., Hemmingsen, L., Penner-Hahn, J. E., and Pecoraro, V. L. (2002) Comparison of the binding of cadmium(II), mercury(II), and arsenic(III) to the *de novo* designed peptides TRI L12C and TRI L16C, *J. Am. Chem. Soc. 124*, 8042−8054.
14. Farrer, B. T., Harris, N. P., Balchus, K. E., and Pecoraro, V. L. (2001) Thermodynamic model for the stabilization of trigonal thiolato mercury(II) in designed three-stranded coiled coils, *Biochemistry 40*, 14696−14705.
15. Ghosh, D., and Pecoraro, V. L. (2004) Understanding metalloprotein folding using a *de novo* design strategy, *Inorg. Chem. 43*, 7902−7915.
16. Chan, W. C., and White, P. D. (2000) Fmoc solid-phase peptide synthesis: A practical approach, Oxford University Press, New York.
17. Ellman, G. M. (1959) Tissue sulfhydryl groups**,** *Arch. Biochem. Biophys. 82*, 70.
18. Pace, C. N., and Scholtz, J. M. (1997) Protein structure: A practical approach, Oxford University Press, Oxford, U.K.

19. Boice, J. A., Dieckmann, G. R., Degrado, W. F., and Fairman, R. (1996) Thermodynamic analysis of a designed three-stranded coiled coil, *Biochemistry 35*, 14480−14485.
20. Demeler, B., and van Holde, K. E. (2004) Sedimentation velocity analysis of highly heterogeneous systems, *Anal. Biochem. 335*, 279−288.
21. Durchschlag. H. (1986) *Thermodynamic Data for Biochemistry and Biotechnology* (Hinz, H.-J., Ed.) Springer-Verlag, New York.
22. Dieckmann, G. R., McRorie, D. K., Lear, J. D., Sharp, K. A., DeGrado, W. F., and Pecoraro, V. L. (1998) The role of protonation and metal chelation preferences in defining the properties of mercury-binding coiled coils, *J. Mol. Biol. 280*, 897−912.
23. Johnson, M. L., Correia, J. J., Yphantis, D. A., and Halvorson, H. R. (1981) Analysis of data from the analytical ultracentrifuge by nonlinear least-squares techniques, *Biophys. J. 36*, 575−588.
24. Gill S. C., and von Hippel P. H. (1989) Calculation of protein extinction coefficients from amino acid sequence data, *Anal. Biochem. 182*, 319−326.
25. Demeler, B., Saber, H., and Hansen, J. C. (1997) Identification and interpretation of complexity in sedimentation velocity boundaries, *Biophys. J. 72*, 397−407.
26. Utschig, L. M., Wright, J. G., and O'Halloran, T. V. (1993) *Biochemical and Spectroscopic Probes of Hg^{II} Coordination Environments in Protein*, Vol. 226, Academic Press Inc., San Diego, CA.
27. Watton, S. P., Wright, J. G., MacDonnell, F. M., Bryson, J. W., Sabat, M., and O'Halloran, T. (1990) Trigonal mercuric complexes of an aliphatic thiolate: A spectroscopic and structural model for the receptor site in the Hg^{II} biosensor merR, *J. Am. Chem. Soc. 112*, 2824−2826.
28. Shewchuk, L. M., Verdine, G. L., and Walsh, C. T. (1989) Transcriptional switching by the metalloregulatory merR protein: Initial characterization of DNA and mercury(II) binding activities, *Biochemistry 28*, 2331−2339.
29. Matzapetakis, M., Ghosh, D., Weng, T.-C., Penner-Hahn, J., and Pecoraro, V. L. Peptidic models for the binding of Zn^{II}, Pb^{II}, Bi^{II}, and Cd^{II} to mononuclear thiolate binding sites, manuscript in preparation.
30. Farrer, B., McClure, C., Penner-Hahn, J. E., and Pecoraro, V. L. (2000) Arsenic stabilizes three-helix bundles in aqueous solution, *Inorg. Chem. 39*, 5422−5423.
31. Demeler, B. (2005) *UltraScan Version 7.0, a Comprehensive Data Analysis Software Package for Analytical Ultracentrifugation Experiments*, The University of Texas Health Science Center at San Antonio, Department of Biochemistry, San Antonio, TX.
32. Cheesman, B. V., Arnold, A. P., and Rabenstein, D. L. (1988) Nuclear magnetic resonance studies of the solution chemistry of metal complexes. 25. $Hg(thiol)_3$ complexes and Hg^{II}-thiol ligand exchange kinetics, *J. Am. Chem. Soc. 110*, 6359−6364.
33. Shoukry, M. H., Cheesman, B. V., and Rabenstein, D. L. (1988) Polarimetric and nuclear magnetic resonance studies of the complexation of mercury by thiols, *Can. J. Chem. 66*, 3184−3190.
34. Lee, K.-H., Matzapetakis, M., Mitra, S., Marsh, E. N. G., and Pecoraro, V. L. (2004) Control of metal coordination number in *de novo* designed peptides through subtle sequence modifications, *J. Am. Chem. Soc. 126*, 9178−9179.

BI0506674